Biosensors and Bioelectronics 135 (2019) 181–191

Contents lists available at ScienceDirect

Biosensors and Bioelectronics

journal homepage: www.elsevier.com/locate/bios

Flexible bioelectrodes with enhanced wrinkle microstructures for reliable electrochemical modification and neuromodulation in vivo

Bowen Ji[a,1], Minghao Wang[a,1], Chaofan Ge[b], Zhaoqian Xie[c,d], Zhejun Guo[a], Wen Hong[a], Xiaowei Gu[b], Longchun Wang[a], Zhiran Yi[a], Chunpeng Jiang[a], Bin Yang[a], Xiaolin Wang[a], Xiuyan Li[a], Chengyu Li[b], Jingquan Liu[a,*]

[a] National Key Laboratory of Science and Technology on Micro/Nano Fabrication, Department of Micro/Nano Electronics, Shanghai Jiao Tong University, Shanghai, 200240, China

[b] Institute of Neuroscience and Key Laboratory of Primate Neurobiology, Shanghai Institutes for Biological Sciences, Chinese Academy of Sciences, Shanghai, 200031, China

[c] Department of Engineering Mechanics, Dalian University of Technology, Dalian, 116024, China

[d] Department of Civil and Environmental Engineering, Mechanical Engineering, and Materials Science and Engineering, Northwestern University, Evanston, IL, 60208, USA

ARTICLE INFO

Keywords:
Flexible bioelectrodes
Enhanced wrinkle microstructures
Electrochemical modification
ECoG recording
Optogenetics stimulation

ABSTRACT

Limited electrode size with high electrochemical performance and reliability of modified materials are two of the main concerns for flexible neural electrodes in recent years. Here, an effective fabrication method of enhanced micro-scale wrinkles based on oil-pretreated hyperelastic substrates (PDMS and Ecoflex) is proposed for the application of microelectrode biosensors. Compared to pre-stretching or compressing methods, this approach has better advantages including compatibility with MEMS processes on wafer and easy replication. Wrinkled gold microelectrodes exhibit superior electrochemical properties than the flat one, and no crack or delamination occurs after electroplating PEDOT:PSS and platinum black on wrinkled microelectrodes. Cyclic voltammetry (CV) scanning for 2500 times is performed to investigate adhesion and stability of modified materials. For the modified microelectrodes, no significant change is observed in charge storage capacity (CSC) and impedance at 1 kHz, whereas PEDOT:PSS coated flat microelectrodes appears delamination. Ultrasonication and cycling forces are also conducted on modified microelectrodes, which demonstrates little influence on the wrinkled ones. Flexible wrinkled microelectrodes are further verified by in-vivo ECoG recordings combined with optogenetics in mice. These results highlight the importance of micro-structure in neural electrode design and tremendous application potentials in flexible electronics.

1. Introduction

The advent of flexible electrode as neural interface has been an exciting field in neuroscience and bioelectronics. Electrophysiological electrodes with high-performance electrochemical, mechanical and biological characteristics play a crucial role in the advanced neural interface with soft tissues, especially for the implantation occasions. Generally, microelectrodes are fabricated on flat substrates, like polyimide (PI), Parylene-C, polyethylene terephthalate (PET) and poly (dimethyl siloxane) (PDMS) film. Meanwhile, the electrode modification with poly (3,4-ethylenedioxythiophene) (PEDOT) (Ludwig et al., 2006), platinum black (Pt-black) (Rui et al., 2011), iridium oxide (IrO_x) (Weiland and Anderson, 2000) or carbon nanotube (CNT) (Wang et al., 2006), etc. is indispensable to improve electrode performance during signal recordings. However, these microelectrodes are limited by their inherent area size, especially for the occasion with urgent need of satisfying performance on tiny size. Hence, the surface morphology from 2D to 3D can provide a path to address this issue.

A new way of improving active surface area is roughening the surface, like crumpled or wrinkled 3D surface structures. Wrinkle is a ubiquitous phenomenon observed in many cases and has gained substantial interest in different applications over the past decades. It is generally understood that the wrinkle formation existing on the surface (bending out of plane) is caused by any extrinsic force, such as mechanical stretching or compression, heating, swelling (García-Gallegos et al., 2014; Khang et al., 2009; Bowden et al., 1998), etc. capable of

* Corresponding author. Institute of Micro/Nano Science and Technology, 800 Dong Chuan Road, Shanghai, 200240, PR China.
E-mail address: jqliu@sjtu.edu.cn (J. Liu).

[1] Bowen Ji and Minghao Wang contributed equally to this work.

https://doi.org/10.1016/j.bios.2019.04.025
Received 14 February 2019; Received in revised form 31 March 2019; Accepted 13 April 2019
Available online 17 April 2019
0956-5663/

inducing the stress exceeding a critical value (He et al., 2015). Although several mechanisms can be used to generate wrinkles, the typical model of a soft elastic foundation with a rigid skin on its top surface will be the preferred approach in our study. The top rigid skin has variation in dimension and shapes due to different processes such as stress relaxation, compression, cooling or solvent evaporation if the elastic foundation is swollen. Consequently, the compressive force is created on the rigid skin, generating wrinkles on the top surface (Rodríguez-Hernández, 2015). To date, wrinkles have been applied to design multiple types of electronic devices, including sensors (Park et al., 2018; Nur et al., 2018), actuators (Watanabe et al., 2002), transistors (Graz and Lacour, 2009; Chae et al., 2013), light-emitting diodes (LEDs) (Koo et al., 2010), solar cells (Kim et al., 2012; Bu, 2014), piezoelectric and triboelectric devices (Qi et al., 2011; Uddin and Chung, 2016), supercapacitors (Yu et al., 2009; Chen et al., 2013) and batteries (Sahoo and Ramaprabhu, 2015). However, rare studies of wrinkle application in microelectrodes are reported in literature (Long et al., 2014; Yang et al., 2016) which are mainly based on heating or pre-stretching methods. As is well-known, Parylene-C has been universally used as the structural material in biomedical devices with outstanding properties, such as pinhole-free conformality, chronic biocompatibility as Class VI material, low water permeability, high flexibility and great mechanical strength (Ji et al., 2017). Especially, Parylene-C is widely applied as the flexible substrate for implantable neural electrodes. Even though a few researchers had proposed PDMS-Parylene hybrid electrodes, they did not pay attention on the surface morphology or material modification (Chou et al., 2013; Ochoa et al., 2013; Lee et al., 2017). Therefore, we hope to fabricate electrodes based on the ideal material Parylene-C as well, combining with soft elastic material like PDMS to generate wrinkle features (Takei and Fujita, 2015; Oh et al., 2016).

Here, we propose a new approach to obtain the enhanced micro-scale wrinkles on microelectrodes by oil extraction from the elastic substrate for the first time. This method is based on relatively uncomplicated fabrication routes which is more compatible with wafer-level MEMS technology. By electroplating modified materials poly (3,4-ethylenedioxythiophene): polystyrene sulfonate (PEDOT:PSS) and platinum black (Pt-black) on the wrinkled microelectrode sites, the obtained uniform coatings exhibit promising potentials in electrophysiological measurement with relatively larger effective surface area than the flat one. To investigate the advantages and usability of such microstructures as neural interface, the electrochemical stability and neural recording ability combined with optogenetics in vivo are verified under realistic experimental conditions. We also identify the minor effects of the material and thickness of the elastic substrates (PDMS or Ecoflex) to the bending mechanics by simulation, suggesting comparable flexibility on curved cortical surface. Overall, to the best of our knowledge, the flexible electrode with self-generating enhanced micro-scale wrinkles has rarely been reported, and it exhibits noticeable stability and utility extending to various wearable and implantable sensors which require reliable modification and high resolution.

2. Materials and methods

2.1. Fabrication of the enhanced wrinkled microelectrodes

A 300 nm thick aluminum (Al) was evaporated on silicon wafer by physical vapor deposition as the sacrificial layer. The poly (dimethyl siloxane) (PDMS; 10:1 base: crosslinker by weight; Sylgard 184, Dow Corning, Auburn, MI, USA) and silicone oil (XIAMETER PMX-200 Silicone Fluid, Dow Chemical Company, Mitland, MI, USA) were mixed together with 7:3 wt ratio followed by pumping air bubbles in vacuum drier for 15 min, spin-casting on silicon wafer with speed of 1800 rpm and curing in an oven at 70 °C for 1 h. Similarly, the Ecoflex (00–30, Smooth-On, Macungie, PA, USA) with two components A and B (1:1 wt ratio) were mixed with silicone oil (30% in weight), vacuumed for 5 min, spun on silicon wafer at 1000 rpm and cured at room temperature for 4 h to produce the elastic substrate. The cured PDMS and Ecoflex substrates were equally about 20 μm in thickness. To fully extract the silicone oil from PDMS and Ecoflex, they were both soaked in the organic chloroform bath for more than 12 h followed by rinsing with deionized water.

The following processes were the same for both elastic substrates. A first layer of 5 μm Parylene-C film was deposited in PDS2010 system (Specialty Coating Systems, USA). Then, a 30/300 nm Cr/Au layer was sputtered with pretreatment of oxygen plasma of Parylene-C for 1 min. A 3 μm thick layer of positive photoresist was spun, photoetched and post baked. The metal layer was patterned in the ion beam etching system with Ar gas. Immersion in acetone for 1 h removed the residual photoresist. Here, the metal patterning could not be realized by wet etching due to the etchant undercutting from the rugged side wall of metal leads. O_2 plasma was then applied for 2 min (80 W RF power) to activate the surface of underlying Parylene-C to enhance the adhesion of the subsequent top Parylene-C layer. Next, another layer of 5 μm Parylene-C film was deposited followed by spin-casting a 15 μm thick layer of photoresist and photoetching to define the microelectrode sites and outline. Reactive-ion etching (RIE) was applied at 300 mTorr and 80 W with 20 sccm O_2 for 30 min to remove the top Parylene-C encapsulant at microelectrode sites and pads. An additional photoresist was spun at 1000 rpm as a protective layer during the UV laser cutting of the elastic PDMS or Ecoflex as the outline of the Parylene-C film above. After removing the photoresist in acetone, the wafer was immersed in hydrochloric acid solution (HCl:H2O = 1:5) to fully undercut Al sacrificial layer and release devices. Flatting the device on the non-sticky Teflon tape helped the paste printing on pads. A 20 μm stainless steel sheet was patterned by UV laser method, aligned to the pad area and used as a mask to print the silver paste. A flexible flat cable (FFC) was fixed on the glass slide with conductor side upwards. The pads covered with silver paste on Teflon tape were aligned and stuck to the FFC conductor followed by placing a weight on top under 120 °C in oven for 3 h. Finally, the interface to FFC was carefully encapsulated with a drop of epoxy resin and the Teflon tape was removed easily.

2.2. Electrochemical deposition and characterization

2.2.1. Electrodeposited PEDOT:PSS electrodes

Firstly, 5 mg/ml Polystyrene sulfonate (PSS) powder was added to 50 ml deionized water and stirred to dissolve. Then, 0.01 M EDOT was added and the solution was mixed uniformly by using a stir bar for 2 h to obtain the electrolyte. Prior to the PEDOT: PSS electrodeposition, 50 C V cycles were performed on all channels from −1.0–1.0 V versus saturated calomel electrode (SCE) with 1 V/s scanning rate in phosphate buffered saline (PBS, pH 7.4) as a cleaning step. The PEDOT: PSS composite was electrodeposited by the galvanostatic method in a three-electrode cell with the fabricated electrode sample as the working electrode, Pt mesh as a counter electrode and SCE as a reference electrode. The deposition was carried out on an electrochemical workstation (CHI 660c, CH Instruments Inc., USA) by applying a constant current with deposition current density of 0.4 mA/cm^2 for 10 min. To ensure the same plating thickness for quantitative comparison, the electrodes based on flat Parylene-C, PDMS_oil and Ecoflex_oil used their own effective surface areas to calculate the current values during electrodeposition.

2.2.2. Electrodeposited Pt-black electrodes

The electrode sites were electroplated Pt-black by applying a repetitive current pulse train (5:500 ms duty ratio, 4.5 A/cm^2 peak current density, 300 cycles) in chloroplatinic acid solution (H2PtCl6, 3% chloroplatinic acid and 0.01% lead acetate in deionized water) with a gold rod as both counter and reference electrodes in ultrasonic bath (50 W, 40 kHz). The same methods were used to clean the electrode surface and calculate the respective currents for electrodes with different effective surface areas.

2.2.3. Electrochemical characterization

Both cyclic voltammetry (CV) and electrochemical impedance spectroscopy (EIS) were measured using a standard three electrodes system (PGSTAT12 Autolab, EcoChemie, Utrecht, Netherlands) with a Pt sheet as a counter electrode and SCE as a reference electrode in PBS. CV was scanned over the potential range of −0.6 V and 0.8 V at the scanning rate of 100 mV/s. EIS was measured at frequency range of 0.1 Hz–100 kHz with AC excitation voltage amplitude of 10 mV at open circuit potential (OCP).

2.3. Mechanics simulations

The commercial software ABAQUS (Hibbitt et al., 2010) enabled the conventional static analysis to stimulate the bending processes with and without hyperelastic substrates. Eight-node 3D solid elements (C3D8R) and four-node shell elements (S4R) were used to model the hyperelastic substrate (PDMS or Ecoflex) and rigid film (Parylene-C), respectively. The computational accuracy can be ensured by the convergence of mesh sizes. For FEA results presented in Fig. S9, the elastic-plastic transition of Au was set when the maximum strain of half the width of one section was beyond the yield strain of 0.3%. The Young's modulus (E) and Poisson's ratio (ν) are E_{PDMS} = 1 MPa and ν_{PDMS} = 0.49 for PDMS; $E_{Ecoflex}$ = 60 kPa and $\nu_{Ecoflex}$ = 0.49 for Ecoflex; E_{PAC} = 3.2 GPa and ν_{PAC} = 0.40 for Parylene-C; E_{Cr} = 279 GPa and ν_{Cr} = 0.21 for Cr; E_{Au} = 79 GPa and ν_{Au} = 0.42 for Au.

The effective bending stiffness EI of the layered structure of the flexible electrode is given by (Su et al., 2014)

$$EI = \sum_{i=1}^{n} E_i h_i \left\{ \frac{h_i^2}{3} + \left[\left(\sum_{j=1}^{i} h_j \right) - \left(\sum_{j=1}^{i} h_j \right) - h_{neutral} \right]^2 - h_i \left[\left(\sum_{j=1}^{i} h_j \right) - \left(\sum_{j=1}^{i} h_j \right) - h_{neutral} \right] \right\} \quad (1)$$

where the summation is for all n layers with i = 1 being the bottom layer. E_i and h_i are Young's modulus and thickness of i^{th} layer. The distance $h_{neutral}$ from the bottom to the neutral mechanical plane of the cross section is given by

$$h_{neutral} = \frac{\sum_{i=1}^{n} E_i h_i \left[\left(\sum_{j=1}^{i} h_j \right) - \frac{h_i}{2} \right]}{\sum_{i=1}^{n} E_i h_i} \quad (2)$$

2.4. Animal procedures

All experimental procedures were performed in accordance with the guidelines established by Animal Care and Us Committee of the Institute of Neuroscience, Chinese Academy of Sciences, Shanghai, China. VGAT-Cre transgenic mouse (12 weeks, weighted ~25 g) expressing AAV-DIO-ChR2 virus was used for the acute experiment. An awake mouse was head-fixed by a plate to the fixing bar. A left rectangular parietal craniotomy was made with a surgical drill and the bone flap was separated with a microdissector. Then, the durotomy in x-shape was achieved by lifting the dura mater with microforceps and cutting with a pair of microscissors. Approximately 2.5 × 2.5 mm^2 cranial window was made exposing the area across the somatomotor cortex and somatosensory cortex. The electrode was placed on the exposed subdural cortical surface and keep in good state with a slurry of gelfoam and artificial cerebrospinal fluid (ACSF). A skull screw was placed in the right frontal bone to serve as the reference electrode for the recordings, and the ground was connected to the plate fixed on the skull. Once experimentation was completed, the mouse was killed immediately with an intraperitoneal injection of pentobarbital solution.

2.5. Neural signal recording and analysis

ECoG signals from four channels were amplified and digitized at a sampling rate of 1 kHz with the Multichannel Acquisition Processor (Plexon Inc, USA). The data were processed in EEGLAB package (Magri et al., 2009) with frequency pass band 0.5–200 Hz. To eliminate or reduce the impact of power frequency interference, all electric sources in the surroundings were powered off during recording.

2.6. Optogenetic stimulation

An optical fiber (200 μm in diameter, NA: 0.37) was connected to the blue diode pumped solid state laser (473 nm) and fixed with 2 mm distance from the fiber tip to the electrode. The laser power at the tip of fiber was measured with a laser power meter (LP1, Sanwa Electric Instrument Ltd, Japan). A series of 10 s stimulations of blue light was delivered with frequency of 1 Hz, pulse width of 5 ms and intensity of 8 mW.

3. Results and discussion

3.1. Design and fabrication of the enhanced wrinkled microelectrodes

Obvious isotropic surface wrinkling is formed by the residual stress when depositing the Parylene-C film (Young's moulus E = 3.2 GPa) on the PDMS (E = 1.0 MPa) or Ecoflex (E = 60 kPa) elastic substrate which is pretreated by mixing and extracting moderate silicone oil. Fig. 1A showed the structure of the wrinkled microelectrodes consisting of the oil-pretreated PDMS or oil-pretreated Ecoflex substrate (20 μm), bottom insulating Parylene-C film (5 μm), Cr/Au (30/300 nm) electrode layer, top encapsulating Parylene-C film (5 μm) and modified electrode coating PEDOT:PSS or Pt-black. Hereafter, the oil-pretreated PDMS and oil-pretreated Ecoflex substrates were referred to as simply “PDMS_oil” and “Ecoflex_oil”, respectively. The basic formation principle of the enhanced surface wrinkle was illustrated in Fig. 1B. The controlled stoichiometric addition of silicon oil into the uncured PDMS or Ecoflex acted as a molecularly dispersed filler. The elastic substrate on the wafer emerged in-plane shrinkage due to the diffusion of silicone oil into the chloroform solvent, which gave rise to the embedded in-plane stress. Here, the volume fraction of oil in the composition determined the degree of embedded stress (Egunov et al., 2016). Furthermore, the amplitude of the wrinkles was directly related to the intensity of the embedded stress. When a rigid skin layer (Parylene-C) was deposited on the elastic substrate, the stress relaxation in the substrate further facilitated the formation of compressive stress on the skin, which was the main cause of the enhanced surface wrinkles. As for the elastic substrates without oil-pretreatment, low or unobservable amplitude fluctuation could be seen after Parylene-C deposition (Fig. S1). Fig. 1C showed the basic MEMS fabrication approach employed in this study as previously mentioned. In view of the crack phenomenon of metal pads when hot pressed to flexible flat cable (FFC) via anisotropic conductive film (ACF), the silver paste was applied to electrode pads for reliable connection to FFC as pictured in Fig. S2. Due to the slight spread of silver paste during hot pressing, the openings on the stainless-steel mask should be smaller than the exposed pads of the device.

3.2. Characteristic enhanced wrinkle microstructures

Optical inspection of the fabricated device before and after encapsulation in Fig. 2A indicated the size of the substrate with the width of 2.3 mm and length of 15 mm. In this study, focus was on the electrode sites with diameter of 200 μm. Optical microscope pictures of the micro-wrinkle structures based on PDMS_oil and Ecoflex_oil were shown in Fig. 2B. Surface wrinkle amplitudes were measured by a digital microscope (Fig. 2C) with the maximum of 3.05 μm for PDMS_oil and 7.84 μm for Ecoflex_oil. However, the optical or digital microscope

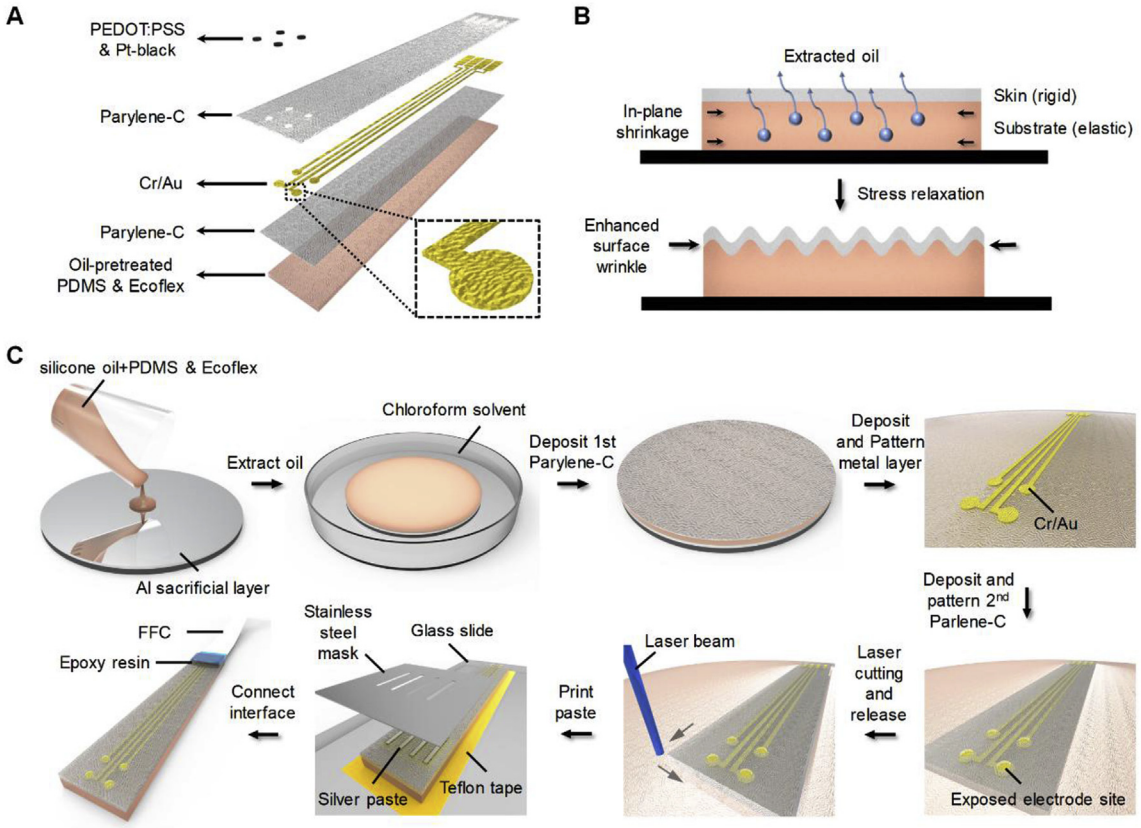

Fig. 1. Enhanced wrinkled microelectrodes formed by depositing rigid Parylene-C film on the oil-pretreated elastic substrate. (A) Exploded view of the layout. (B) Basic formation principle of the enhanced surface wrinkle. (C) Schematic illustration of the fabrication processes of the microelectrodes for neural recordings on the cerebral cortex of mice.

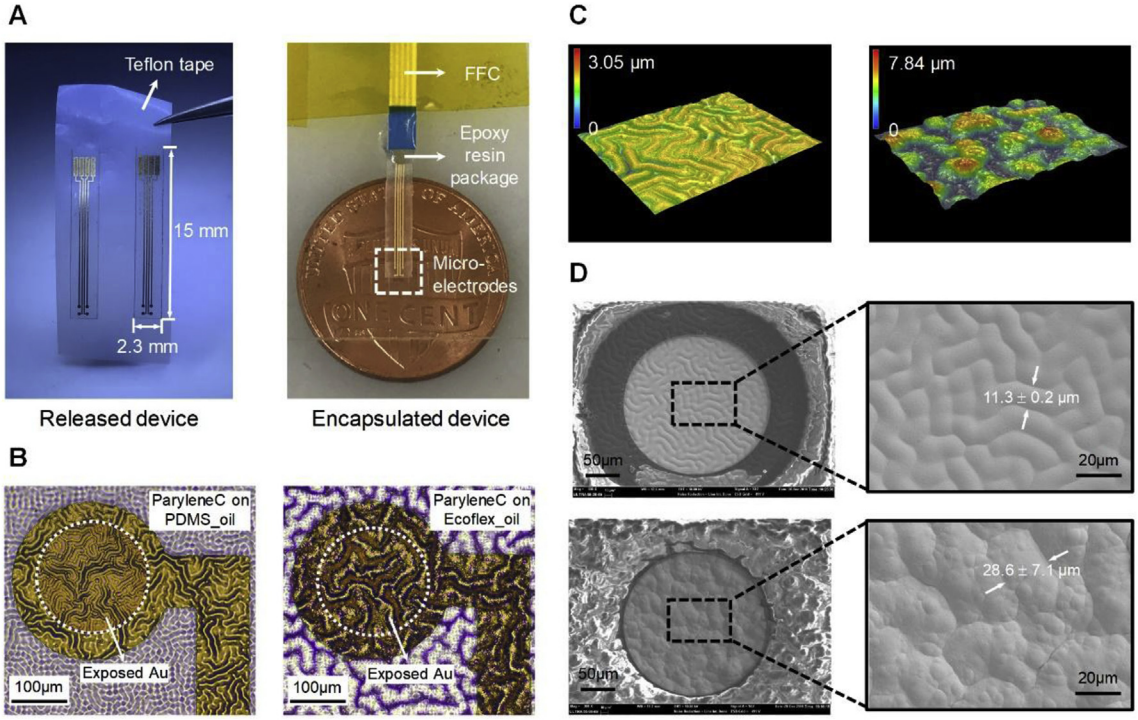

Fig. 2. Fabricated device and the characteristic micro-wrinkle structures on PDMS_oil and Ecoflex_oil. (A) Picture of the released device and its encapsulated state. (B) Optical images of the micro-wrinkle structures (left: PDMS_oil substrate; right: Ecoflex_oil substrate). (C) Surface wrinkle amplitudes measured by digital microscope (left: PDMS_oil substrate; right: Ecoflex_oil substrate). (D) Scanning electron microscope (SEM) pictures illustrating the clean microelectrode sites by adequate reactive ion etching (RIE) treatment and wrinkle wavelengths (top: PDMS_oil substrate; down: Ecoflex_oil substrate).

could not verify the residual of unetched transparent Parylene-C on the electrode sites. Therefore, the scanning electron microscope (SEM) pictures were imperative to demonstrate whether the electrode sites were clean by adequate reactive ion etching (RIE) treatment (Fig. 2D) or not (Fig. S3). Meanwhile, surface wrinkle wavelengths were marked in the zoom-in pictures in Fig. 2D as 11.3 ± 0.2 μm and 28.6 ± 7.1 μm for PDMS_oil and Eccoflex_oil, respectively. Besides, the enlarged SEM picture exhibited omni-distributed bubble structures with the diameters varied from 2.2 to 11.7 μm from the wrinkled microelectrode surface morphology based on Ecoflex_oil (Fig. S4), which further increased the roughness for adhesion promotion of electroplating materials.

3.3. Electrochemical deposition and characterization of the enhanced wrinkled microelectrodes

To investigate the electroplating uniformity on enhanced wrinkled microelectrode sites, two common modification materials of PEDOT:PSS and Pt-black were chosen in this study. PEDOT:PSS has emerged as a superior material for neural interfaces because of its low electrochemical impedance with high signal-to-noise ratio (SNR) for electrophysiological recording, high charge injection capacity for electrical stimulation and compliant mechanical performance for conformal contact to soft tissue (Ganji et al., 2018). Pt-black has a rough surface which is composed of even-distributed cauliflower shape particles with great electrochemical properties, excellent biocompatibility and stability by ultrasonic electroplating (Shi et al., 2012). To ensure the comparability, the same coating thickness are indispensable for microelectrodes with different effective surface areas. Comparison of effective surface areas was made on microelectrode sites with diameter of 200 μm between the flat, PDMS_oil and Ecoflex_oil in Fig. 3A, which were 31416 μm^2, 41946.5 ± 706.4 μm^2 and 44483.2 ± 861.6 μm^2, respectively. The PDMS_oil and Ecoflex_oil substrates exhibited 33.5% and 41.6% larger than the flat one in surface area. The electroplating voltage curve of PEDOT:PSS in galvanostatic mode with constant current in a three-electrode cell was given in Fig. 3B. Fig. 3C showed the potential changing versus time by current pulse electroplating of Pt-black in a two-electrode cell in ultrasonic bath. The magnification of the Pt-black electroplating curve illustrated the repetitive current pulse train (5:500 ms duty ratio, Fig. 3D). The electroplating was processed site by site to guarantee the uniformity of coating on all microelectrode sites. The optical images of wrinkled Au (unmodified), PEDOT:PSS and Pt-black modified microelectrodes on PDMS_oil were presented in Fig. 3E, G and I, illustrating uniform coating of both PEDOT:PSS and Pt-black without cracks or delamination. Meanwhile, the same satisfactory electroplating results could be found from the optical images of wrinkled Au, PEDOT:PSS and Pt-black modified microelectrodes on Ecoflex_oil (see Fig. 3F, H and J), not excepting the trough of wrinkles. It was noteworthy that microelectrode with smaller size (diameter of 100 μm) could also be electrodeposited with homogeneous PEDOT:PSS or Pt-black coating (Fig. S5). However, smaller scale of wrinkles (wavelength) is necessary for smaller size of microelectrodes, which can be controlled by several approaches, such as the thickness of the top rigid layer (Chung et al., 2009), surface modification of the soft substrate (e.g. O_2 plasma, UV-ozone treatment) (Schweikart et al., 2009) and post-annealing (Park et al., 2010).

The results of the electrochemical characterization were summarized in Fig. 4 which showed cyclic voltammogram (CV) and electrochemical impedance spectrum (EIS) diagrams of Au, PEDOT:PSS and Pt-black microelectrodes based on the flat Parylene-C, PDMS_oil and Ecoflex_oil substrates. As shown in Fig. 4A, B and C, the charge storage capacity (CSC) could be extracted from CV curves with the voltage sweep rate of 50 mV/s to quantitatively characterize the amount of charge that could be delivered within the water window (Cogan, 2008). The CSC of original unmodified Au microelectrodes on the flat, PDMS_oil and Ecoflex_oil were 0.58 ± 0.06 mC/cm^2, 1.14 ± 0.08 mC/cm^2 and 1.60 ± 0.11 mC/cm^2, respectively (Fig. 4G). The Au microelectrodes on Ecoflex_oil exhibited greatest charge injection capacity due to the largest effective surface area. As expected, the modified PEDOT:PSS and Pt-black microelectrodes on three different substrates showed similar trends as bare gold with CSC of 13.72 ± 3.41 mC/cm^2, 21.71 ± 4.73 mC/cm^2 and 25.69 ± 6.35 mC/cm^2 for PEDOT:PSS and 51.21 ± 4.71 mC/cm^2, 56.39 ± 5.81 mC/cm^2 and 62.33 ± 8.6 mC/cm^2 for Pt-black, respectively. Compared with the flat microelectrode, the CSC of wrinkled ones on PDMS_oil and Ecoflex_oil exceeded 96.6% and 175.9% for Au, 58.2% and 87.2% for PEDOT:PSS and 10.1% and 21.7% for Pt-black. Fig. 4D, E and F showed the impedance curves at frequency range of 0.1 Hz–100 kHz. The impedances at 1 kHz for Au microelectrodes on the flat, PDMS_oil and Ecoflex_oil were 26.06 ± 0.72 kΩ, 15.20 ± 0.46 kΩ and 10.52 ± 0.31 kΩ, respectively (Fig. 4H). After electrochemical modification, the impedances decreased significantly by one order of magnitude for both PEDOT:PSS and Pt-black. Little difference could be noticed in impedance from the wrinkled electrodes to the flat one. It is due to the relatively large size of the electrode picked. The speed of impedance diminution decreased with the electroplating time and the impedance tended to be stable, which led to minor effects of the effective surface area to impedance between the flat and the wrinkled ones. Taken PEDOT:PSS electroplating on wrinkled PDMS_oil substrate as an example, the impedance had already decreased to 2.18 kΩ at 5 min, then it came to 2.13 kΩ at 10 min. The difference is believed to be greater for the electrode with smaller size. However, such similar low impedance will infinitesimally affect the use in practical neural signal recordings. Besides, the phases at frequency range of 0.1 Hz–100 kHz were compared in Fig. 4I, showing similar curve trends for the same material on the flat and wrinkled surfaces. At 1 kHz, the absolute value of phase decreased significantly from more than 70° of bare gold to 5° nearby after modification.

3.4. Stability of PEDOT:PSS and Pt-black on the enhanced wrinkled microelectrodes

Here, another question arises about whether the electroplated coatings are reliable and durable in practice. To answer this question, the electrochemical stability of electroplated PEDOT:PSS and Pt-black on flat and wrinkled microelectrodes were verified by three ways: 2500 cycles of CV scanning, 1 h of ultrasonication and 1000 cycles of pressure and friction. CV scanning was performed between −0.6 V and 0.8 V in PBS solution with a scanning rate of 1 V/s to assess the stability under electrical stimulation. During the scanning, CV and EIS were measured every 500 cycles and the corresponding CSC and impedance were recorded. Fig. 5A and B showed 72.0%, 44.5% and 50.4% decrement of CSC and 87.3%, 24.2% and 10.0% increment of impedance at 1 kHz after 2500 scanning cycles for the PEDOT:PSS modified microelectrodes on the flat, PDMS_oil and Ecoflex_oil, respectively. Corresponding optical images before and after 2500 scanning cycles were illustrated in Fig. 5C. It was apparent that the delamination of PEDOT:PSS coating happened on the flat substrate, further confirmed by the digital microscope. As a contrast, there was basically no crack, delamination or exfoliation phenomenon for the PEDOT:PSS coatings on the wrinkled substrates. For Pt-black, much smaller changes in CSC and impedance occurred owing to its good stability by ultrasonic electroplating. Fig. 5D and E indicated 16.1%, 11.4% and 7.8% decrement of CSC and 8.8%, 6.2% and 5.6% increment of impedance at 1 kHz after 2500 scanning cycles for the Pt-black modified microelectrodes on three different substrates, respectively. Meanwhile, unobservable changes could be found in the pictures before and after 2500 scanning cycles in Fig. 5F for the flat and wrinkled microelectrodes. The stability was further verified by the ultrasonic impact as well as the simultaneous effects of the pressure and friction on the modified flat and wrinkled microelectrodes. The pressure/friction experiment was conducted on the self-designed biaxial electric platform with a soft

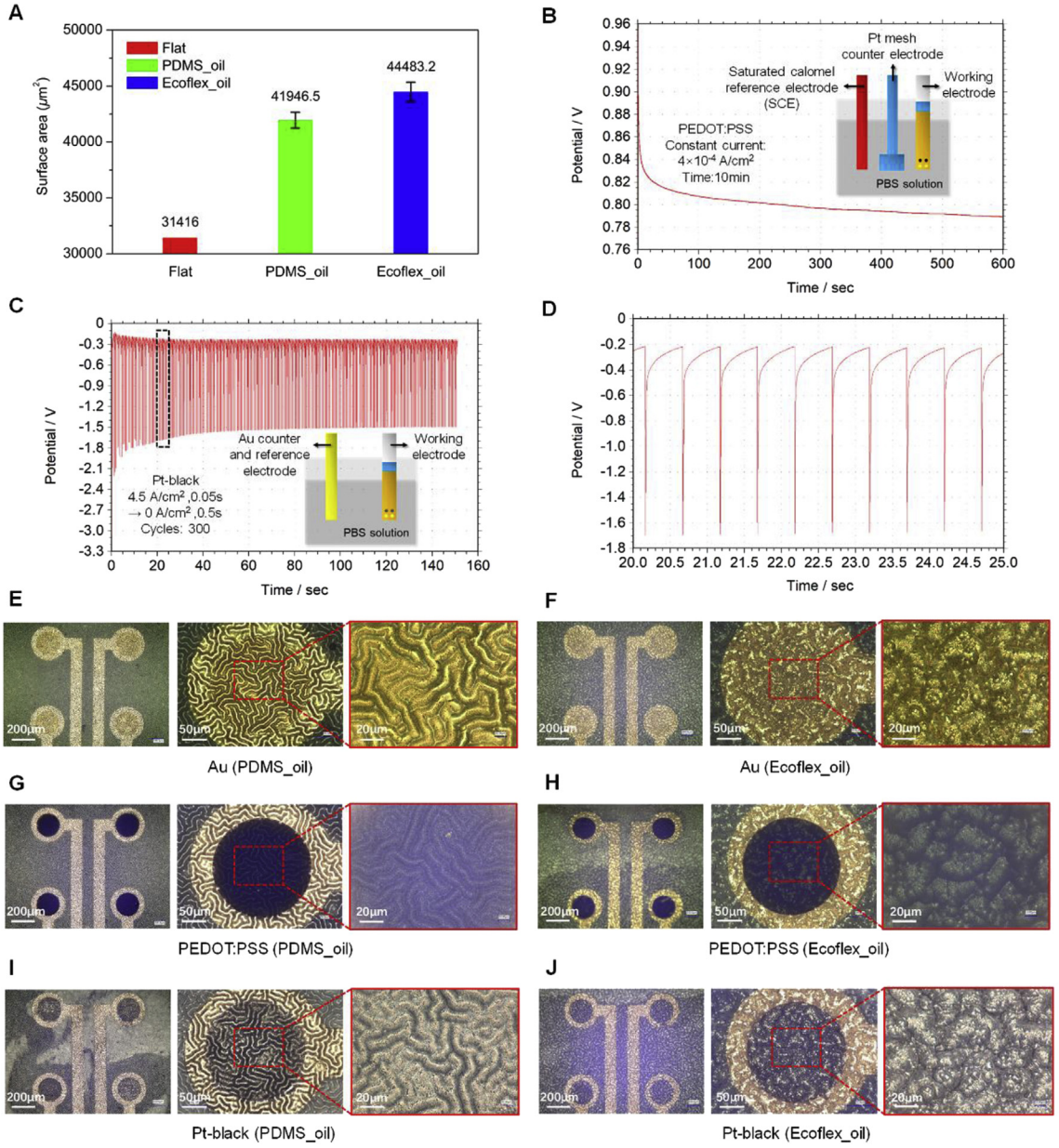

Fig. 3. Electroplating PEDOT:PSS and Pt-black on wrinkled microelectrodes. (A) Comparison of effective surface areas of microelectrode sites (diameter of 200 μm) between the flat, PDMS_oil and Ecoflex_oil. (B) Potential changing versus time by electroplating PEDOT:PSS in galvanostatic mode with constant current in a three-electrode cell. (C) Potential changing versus time by electroplating Pt-black with a repetitive current pulse train in a two-electrode cell, with magnification of the curve (dashed box) (D). Optical images of wrinkled Au (E), PEDOT:PSS (G) and Pt-black (I) microelectrodes on PDMS_oil. Optical images of wrinkled Au (F), PEDOT:PSS (H) and Pt-black (J) microelectrodes on Ecoflex_oil.

polymer-covered (Ecoflex) glass slide fixed on one direction and the electrode sample adhered to the backside of another glass slide moving back and forth on the other direction (Fig. 5G). The Ecoflex film on glass slide maintained compressive state by the glass slide with the electrode sample sandwiched in the middle during reciprocal motion, which provided steady pressure (about 15 kPa) and friction force to the electrode sample. The comparison was made in both CSC and impedance of the original, ultrasonically treated and the one under both pressure and friction in Fig. 5H and I. The inset picture showed the electrode submerged into deionized (DI) water under ultrasonic bath (100 W, 40 kHz). Little change appeared in CSC and impedance after ultrasonication for 1 h, while the impedance slightly increased and the CSC remained well after pressure and friction for 1000 times.

3.5. Mechanics validation of flexibility

Before the in-vivo acute recording to validate the availability of wrinkled microelectrodes, one crucial problem needs to be figured out, whether the wrinkled microelectrodes adding an elastic layer can conformally attach on the curved surface like thin Parylene-C film. Accordingly, a model for computational analysis was made in Abaqus to study the mechanics during bending with and without the elastic PDMS or Ecoflex layer (Fig. S6). The bending area was about $2.3 \times 1.5\ mm^2$ and the deformation was expressed by central angle θ as shown in Fig. S6A and E. Due to the low modulus of elastic layer relative to the rigid Parylene-C layer, the position of neutral plane in the electrode with PDMS or Ecoflex layer kept close to the middle of upper Parylene-C layers, which had little difference with the two-layer Parylene-C electrode, as well as the bending stiffness (Fig. S6C and D). The maximum

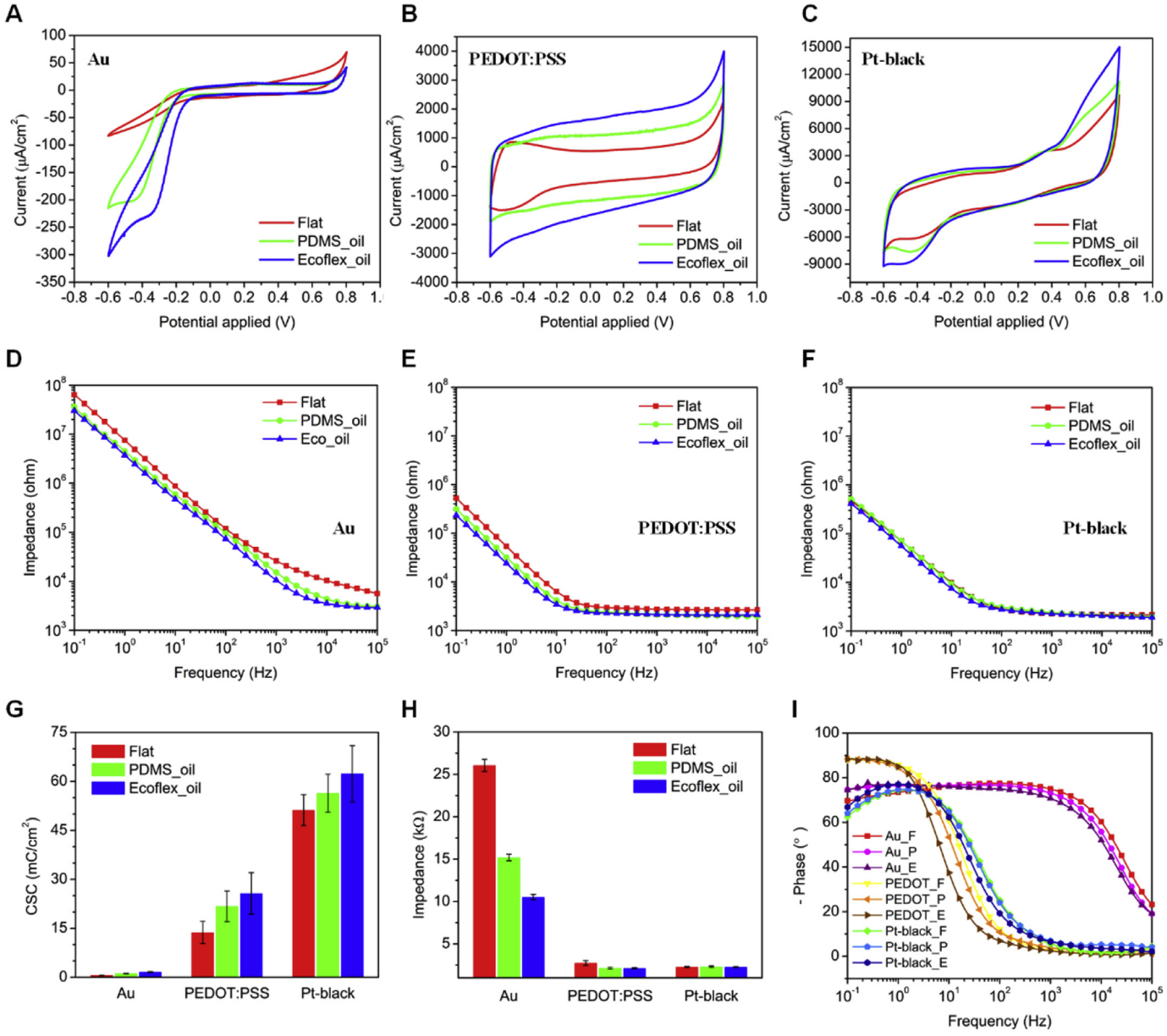

Fig. 4. Electrochemical characterization of Au microelectrodes, PEDOT:PSS and Pt-black modified microelectrodes on flat and wrinkled surfaces. (A–C) CV and (D–F) EIS diagrams of Au, PEDOT:PSS and Pt-black modified microelectrodes between flat Parylene-C, PDMS_oil and Ecoflex_oil. (G) Comparison of CSC values of Au, PEDOT:PSS and Pt-black modified microelectrodes. (H) Comparison of impedances at 1 kHz of Au, PEDOT:PSS and Pt-black modified microelectrodes. The error bars on behalf of standard deviations of three samples with 12 microelectrode sites in total. (I) Comparison of phases at frequency range of 0.1 Hz–100 kHz. Letters F, P and E stand for Flat, PDMS_oil and Ecoflex_oil.

principal strain in Parylene-C layer associated with bending two-layer Parylene-C electrode and the one adding 20 μm PDMS or Ecoflex layer from 45 to 360° was illustrated in Fig. S7 and S8 with little distinction between them. As the thickness of PDMS or Ecoflex layer increased from 20 μm to 40 μm, the maximum principal strain in Parylene-C layer changed little and the influence was mainly concentrated on the maximum strain in the Au layer within the threshold for plastic deformation of 0.3% (Fig. S9 and S10). Consequently, computational results indicated no discernible difference between the two-layer Parylene-C electrode and the one adding elastic layer during bending. The implementable attachment of the wrinkled microelectrodes based on PDMS_oil or Ecoflex_oil on the curved mouse brain further demonstrates the flexibility and conformality of the device.

3.6. In-vivo ECoG recording and optogenetics stimulation with the enhanced wrinkled microelectrodes

To make sure the usability of the wrinkled microelectrodes with PEDOT:PSS and Pt-black coatings, electrocorticogram (ECoG) signals were recorded after electrode implantation on the left cortical surface of an awake transgenic ChR2 mouse as pictured in Fig. 6A. Subdural ECoG can achieve stronger signals by placing electrodes closer to sources than epidural electrodes (Bundy et al., 2015). The electrode was located across the somatomotor cortex and somatosensory cortex as illustrated in Fig. 6B, with an optical fiber (blue light, 473 nm) fixed with 2 mm distance above the electrode for optogenetic stimulation (Fig. S12A and B). ECoG signals were recorded at a sampling rate of 1 kHz and filtered at 0.5–200 Hz during offline analysis, on account of delta (1–3 Hz), theta (4–8 Hz), alpha (8–12 Hz), beta (12–30 Hz) and

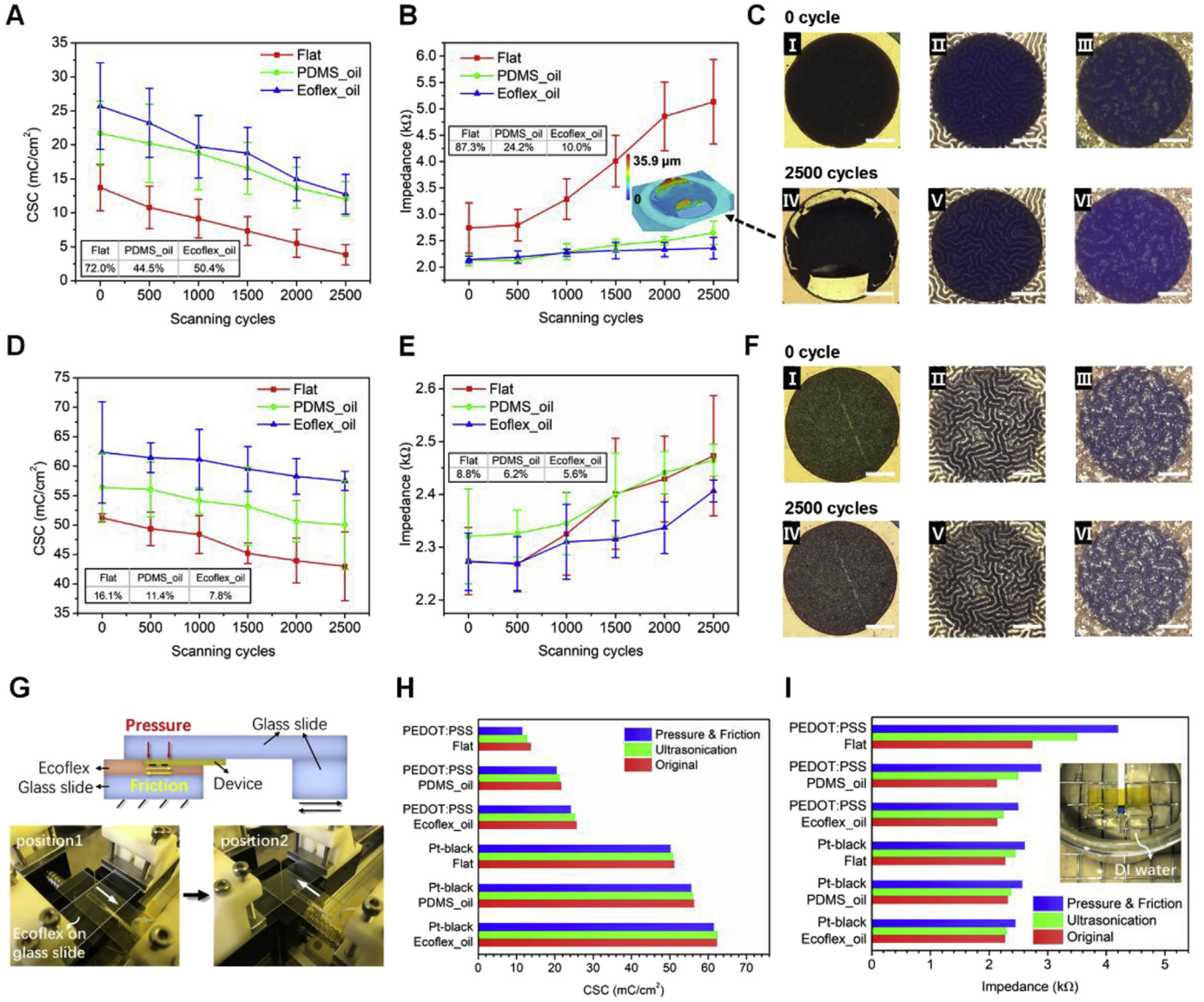

Fig. 5. Electrochemical stability of electroplated PEDOT:PSS and Pt-black on flat and wrinkled microelectrodes with 2500 C V scanning cycles, ultrasonication and 1000 pressure and friction cycles. CSC and EIS with scanning cycles on PEDOT:PSS (A, B) and Pt-black (D, E) modified microelectrodes. The inset tables show the percentage variation of CSC and impedance after 2500 cycles. Pictures of flat (I and IV), PDMS_oil (II and V) and Ecoflex_oil (III and VI) before and after 2500 scanning cycles on PEDOT:PSS (C) and Pt-black (F). The error bars on behalf of standard deviations of three samples with 12 microelectrode sites in total. (G) Illustration and pictures of the pressure/friction experiment on the biaxial electric platform. Comparison of CSC (H) and impedance (I) of the original, ultrasonically treated and the one under both pressure and friction on the PEDOT:PSS and Pt-black modified flat and wrinkled microelectrodes.

gamma (30–80 Hz) band power modulation as dominant signal features, as well as high-gamma (80–200 Hz) activity (Rouse and Moran, 2009; Leuthardt et al., 2012). Taken as an example, four-channel ECoG signals recorded simultaneously by PEDOT:PSS modified wrinkled microelectrodes on PDMS_oil were compared before and after light stimulation (frequency 1 Hz, pulse width 5 ms, intensity 8 mW) in Fig. 6B. Clear low-noise ECoG signals could be acquired by the wrinkled microelectrodes as well as the spikes clearly responded to the light stimulus. A comparison of recorded ECoG signals was made between the unmodified flat Au, PEDOT:PSS and Pt-black modified flat and wrinkled microelectrodes (Fig. S11). Fig. 6C showed the enlarged ECoG signals with intercepted time periods of 20 s (left) and 2 s (right) in a single channel from these seven electrodes. As the impedance of unmodified Au microelectrode was larger than those of PEDOT:PSS and Pt-black modified microelectrodes, ECoG signals recorded by the modified ones showed larger amplitudes. Besides, the unmodified microelectrode exhibited high-level background noise baseline. As a contrast, the noise was decreased significantly after modification with PEDOT:PSS and Pt-black, thus minimizing the amount of non-targeted neural activity picked up in recordings. This might be due to better faradaic charge transfer and capacitive charge coupling of modified materials than the metal one (Ganji et al., 2017). The signal amplitude of Pt-black modified electrodes was relatively larger than the one of PEDOT:PSS. Moreover, the modified wrinkled microelectrodes on both PDMS_oil and Ecoflex_oil exhibited same-level amplitude and similar waveform with the flat one, which efficaciously proved the usability of the winkled microelectrodes in ECoG recordings.

The averaged baseline signal power spectra density (PSD) with error band in four channels was calculated from 120 s of neural activities recorded by unmodified Au, PEDOT:PSS and Pt-black modified flat and wrinkled microelectrodes as a function of frequency (Fig. 6D). The partial enlarged curves illustrated the comparison of power frequency interferences at 50 Hz. It was noted that the spectra of PEDOT:PSS and Pt-black modified microelectrodes showed stronger power than Au

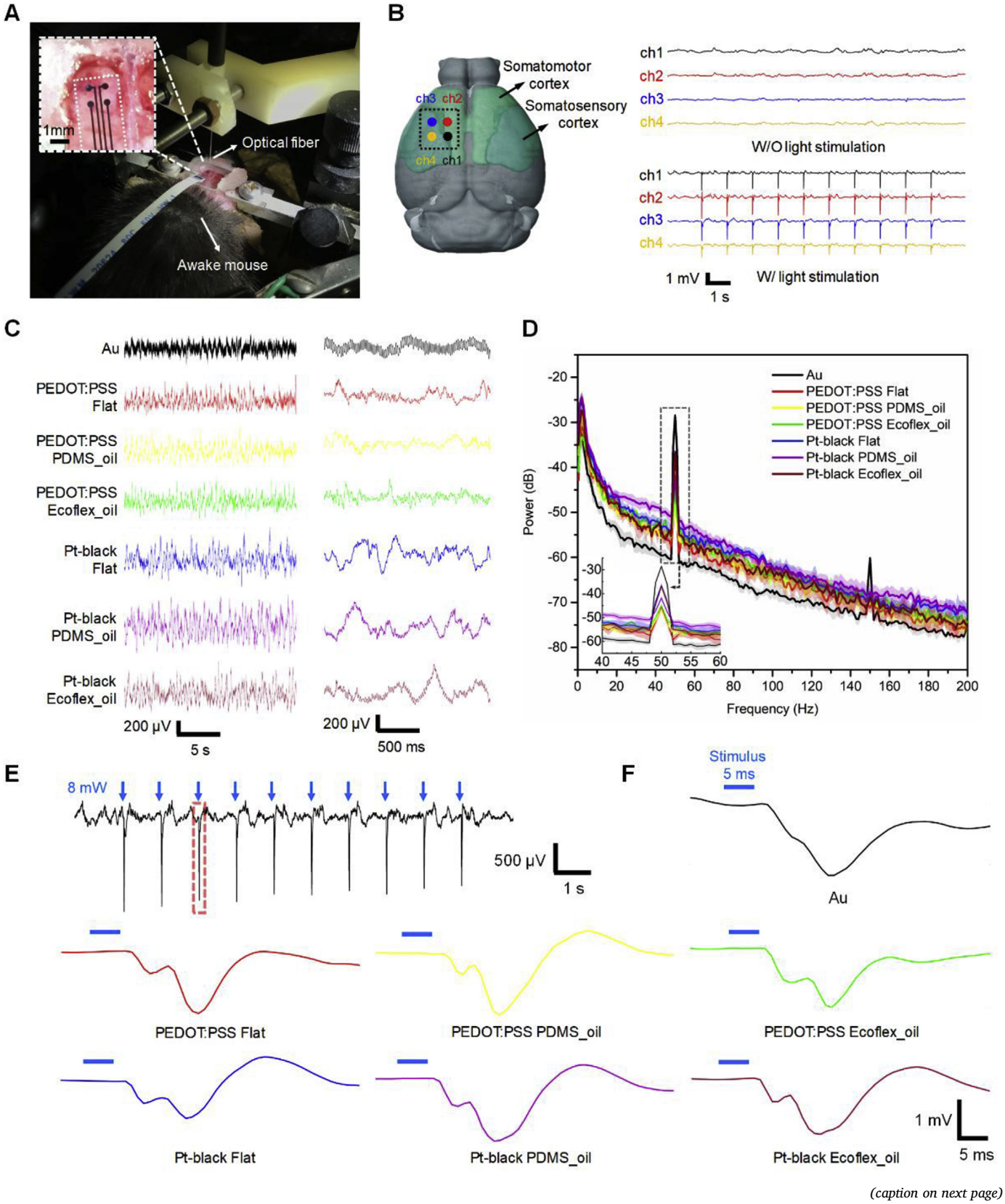

(caption on next page)

microelectrode across the whole frequency range from 0.5 to 200 Hz except for the low power frequency interferences at 50 Hz and 150 Hz, and exhibited higher ECoG sensitivity and common-mode noise suppression capability than Au. Besides, the measured PSD of Pt-black was slightly higher than PEDOT:PSS for both the flat and wrinkled microelectrodes, while both the modified wrinkled microelectrodes based on PDMS_oil and Ecoflex_oil had similar PSD with the flat one. During the acute implantation, stable ECoG signals were observed when we attached and removed the same wrinkled modified electrode on the cortical surface for more than ten times, which demonstrated the

Fig. 6. In vivo neural activity modulation on the cortical surface of mouse. (A) Optical image of wrinkled microelectrodes conformally attached on the exposed cortex of mouse brain. The almost-transparent electrode substrate is highlighted by the white dashed outline in the inset. (B) Illustration of the electrode position (black dashed line) across the somatomotor and somatosensory cortices of mouse brain with four channels. The ECoG signals recorded by PEDOT:PSS modified wrinkled microelectrodes are compared before and after light stimulation with an optical fiber (blue light, 473 nm). (C) Comparison of recorded ECoG signals by unmodified Au (control), PEDOT:PSS and Pt-black modified flat and wrinkled microelectrodes. The intercepted time periods are 20 s (left) and 2 s (right), respectively. (D) Averaged baseline signal power spectra in four channels calculated from 120 s of neural activity recorded by Au (control), PEDOT:PSS and Pt-black modified flat and wrinkled microelectrodes at frequency range from 0.5 to 200 Hz. The partial enlarged curves illustrate the comparison of power frequency interferences at 50 Hz. (E) Representative trace of light-induced ECoG signal with ten light pulses (1 Hz, 8 mW). The blue arrow points to the position of light pulse. (F) Single excited potential responding from Au (control), PEDOT:PSS and Pt-black modified flat and wrinkled microelectrodes. The blue line indicates 5 ms stimulus duration. (For interpretation of the references to colour in this figure legend, the reader is referred to the Web version of this article.)

consistency of recording and stability of modification materials.

To further validate the effectiveness of wrinkled microelectrodes combined with optogenetics, a sequence of 1 Hz, 5 ms, 473 nm light pulse was applied above the unmodified Au, PEDOT:PSS and Pt-black modified flat and wrinkled microelectrodes attached on the same target area. Representative trace of light-induced ECoG signal with ten light pulses was shown in Fig. 6E. Fig. S12 illustrated the time-frequency spectral analysis of the time series ECoG data during the light stimulation. As can be seen, a periodical rapid increase in spectral power was observed along with the light-induced spikes during recording. However, as is known to all, the metal-based microelectrodes suffer from light-induced artefacts (Mikulovic et al., 2016; Thunemann et al., 2018), which are derived from photovoltaic (Becquerel effect) and photothermal effects and appear as transients or oscillations in recordings to interfere with neural recordings. Meanwhile, the frequency, intensity and duration of the light stimulus will affect the amplitude and duration of the artefacts. Here, individual optical evoked potentials (time range 50 ms) responding from Au (control), PEDOT:PSS and Pt-black modified flat and wrinkled microelectrodes were compared in Fig. 6F. Taken the electrical pulse elicited by the light impingent on PEDOT:PSS modified microelectrode site on PDMS_oil as a subject, the artefact induced by photovoltaic effect stood as the initial peak about 5 ms following the light stimulus, and the evoked neural response peak had latency about 11 ms after the stimulus (Fig. S13). The similar results could be investigated in PEDOT:PSS modified flat and wrinkled microelectrodes based on Ecoflex_oil, as well as Pt-black modified flat and winkled microelectrodes based on PDMS_oil and Ecoflex_oil. Thus, artefacts can be distinguished from the evoked neural responses by different temporal electrical features (Park et al., 2014; Ledochowitsch et al., 2015). To eliminate or mitigate artefacts, the graphene (Thunemann et al., 2018), indium tin oxide (ITO) (Ledochowitsch et al., 2015) and CNT (Zhang et al., 2018) etc. can be alternative options on the wrinkled microelectrodes owing to the compatible MEMS processes on wafer. Overall, the initial in-vivo acute animal experiment demonstrated the recording ability of newly developed flexible electrodes with enhanced micro-scale wrinkles on the surface, exhibiting promising potentials in long-term implantation.

4. Conclusions

In summary, we developed a novel method to fabricate microelectrodes with enhanced micro-scale wrinkles by oil extraction from the elastic substrate. As a result, PDMS_oil and Ecoflex_oil substrates exhibit 33.5% and 41.6% larger than the flat one in surface area. We believe this approach has high scalability in wrinkle amplitude, wavelength and patterns, as well as microelectrode size and density depending on the targeted brain regions and applications extended to flexible electronics. We found uniform and stable coatings of both PEDOT:PSS and Pt-black electroplating on the wrinkled microelectrode sites without any cracks, delamination or exfoliation. The electrochemical properties of wrinkled microelectrodes remained better than the flat one after CV scanning cycles for 2500 times, ultrasonication for 1 h, as well as pressure and friction cycles for 1000 times. The animal experiment showed equivalent ECoG signal recording ability of wrinkled microelectrodes with the flat one on PEDOT:PSS and Pt-black, and they could be combined with optical fiber as reliable optogenetics tools. Owing to the rapid development of brain science, this study provides an alternative state-of-the-art fabrication approach to brain-computer interface (BCI) and paves the way to highly reliable and high-performance electronic devices capable of neuroscience exploration and treatment of neurological diseases. The limitation of the enhanced wrinkled microelectrodes exists in the limited increase of the effective surface area, which will be further controlled and improved by different mixtures in liquid elastic polymer, thickness of top rigid layer and pretreatments on the elastic polymer surface in our future work. Flexible electrodes with enhanced wrinkles not only can be used to improve the effective surface area and stability of modified coating, but also can be extended to wearable strain sensor, pressure sensor or energy harvester with high sensitivity and high electrical outputs.

CRediT authorship contribution statement

Bowen Ji: Conceptualization, Methodology, Validation, Writing - original draft. **Minghao Wang:** Methodology, Validation, Writing - review & editing. **Chaofan Ge:** Methodology, Validation. **Zhaoqian Xie:** Methodology, Validation. **Wen Hong:** Validation. **Xiaowei Gu:** Methodology. **Longchun Wang:** Validation. **Zhiran Yi:** Validation. **Chunpeng Jiang:** Writing - review & editing. **Bin Yang:** Writing - review & editing. **Xiaolin Wang:** Writing - review & editing. **Xiuyan Li:** Writing - review & editing. **Chengyu Li:** Supervision, Resources. **Jingquan Liu:** Funding acquisition, Writing - review & editing, Project administration.

Acknowledgements

This work was partially funded by the National Key R&D Program of China under grant 2017YFB1002501, the Natural Science Foundation of China (No. 61728402), Research Program of Shanghai Science and Technology Committee (17JC1402800), Program of Shanghai Academic/Technology Research Leader (18XD1401900). The authors are also grateful to the Center for Advanced Electronic Materials and Devices (AEMD) of Shanghai Jiao Tong University as well as Prof. Yonggang Huang's joint supervision when B. J. stayed in Northwestern University.

Appendix A. Supplementary data

Supplementary data related to this article can be found at https://doi.org/10.1016/j.bios.2019.04.025.

References

Bowden, N., Brittain, S., Evans, A.G., Hutchinson, J.W., Whitesides, G.M., 1998. Nature 393 (6681), 146.
Bu, I.Y.Y., 2014. Mater. Lett. 122, 55–57.
Bundy, D.T., Zellmer, E., Gaona, C.M., Sharma, M., Szrama, N., Hacker, C., Freudenburg, Z.V., Daitch, A., Moran, D.W., Leuthardt, E.C., 2015. J. Neural Eng. 11 (1), 016006.
Chae, S.H., Yu, W.J., Bae, J.J., Duong, D.L., Perello, D., Jeong, H.Y., Ta, Q.H., Ly, T.H., Vu, Q.A., Yun, M., Duan, X., Lee, Y.H., 2013. Nat. Mater. 12 (5), 403.
Chen, T., Xue, Y., Roy, A.K., Dai, L., 2013. ACS Nano 8 (1), 1039–1046.
Chou, N., Yoo, S., Kim, S., 2013. IEEE Trans. Neural Syst. Rehabil. 21 (4), 544–553.
Chung, J.Y., Nolte, A.J., Stafford, C.M., 2009. Adv. Mater. 21 (13), 1358–1362.

Cogan, S.F., 2008. Annu. Rev. Biomed. Eng. 10, 275–309.
Egunov, A.I., Korvink, J.G., Luchnikov, V.A., 2016. Soft Matter 12 (1), 45–52.
Ganji, M., Elthakeb, A.T., Tanaka, A., Gilja, V., Halgren, E., Dayeh, S.A., 2017. Adv. Funct. Mater. 27 (42), 1703019.
Ganji, M., Hossain, L., Tanaka, A., Thunemann, M., Halgren, E., Gilja, V., Devor, A., Dayeh, S.A., 2018. Adv. Healthc. Mater. 7 (22), 1800923.
García-Gallegos, J.H., Nieto-Navarro, J.G., Araujo-Palomo, E.E., Zamora-Antuñano, M.A., Olivares-Ramírez, J.M., Encinas, A., 2014. Mater. Lett. 115, 100–102.
Graz, I.M., Lacour, S.P., 2009. Appl. Phys. Lett. 95 (24), 326.
He, L., Tang, C., Xu, X., Jiang, P., Lau, W.M., Chen, F., Fu, Q., 2015. Surf. Coating. Technol. 261, 311–317.
Hibbitt, Karlsson, Sorensen, 2010. ABAQUS Analysis User's Manual. Pawtucket, RI, USA. vol. 6. pp. 10.
Ji, B., Kang, X., Wang, M., Bao, B., Tian, H., Yang, B., Chen, X., Wang, X., Liu, J., 2017. In: IEEE 30th Int. Conf. on MEMS, pp. 538–541.
Khang, D.Y., Rogers, J.A., Lee, H.H., 2009. Adv. Funct. Mater. 19 (10), 1526–1536.
Kim, J.B., Kim, P., Pégard, N.C., Oh, S.J., Kagan, C.R., Fleischer, J.W., Stone, H.A., Loo, Y.L., 2012. Nat. Photon. 6 (5), 327.
Koo, W.H., Jeong, S.M., Araoka, F., Ishikawa, K., Nishimura, S., Toyooka, T., Takezoe, H., 2010. Nat. Photon. 4 (4), 222.
Ledochowitsch, P., Yazdan-Shahmorad, A., Bouchard, K.E., Diaz-Botia, C., Hanson, T.L., He, J.W., Seybold, B.A., Olivero, E., Phillips, E.A.K., Blanche, T.J., Schreiner, C.E., Hasenstaub, A., Chang, E.F., Sabes, P.N., Maharbiz, M.M., 2015. J. Neurosci. Methods 256, 220–231.
Lee, W.R., Im, C., Koh, C.S., Kim, J.M., Shin, H.C., Seo, J.M., 2017. In: IEEE 39th Int. Conf. on EMBC, pp. 1093–1096.
Leuthardt, E.C., Pei, X., Breshears, J., Gaona, C., Sharma, M., Freudenberg, Z., Barbour, D., Schalk, G., 2012. Front. Hum. Neurosci. 6 (2), 99.
Long, H., Shi, T., Xi, S., Wu, F., Xia, Q., Li, X., Tang, Z., 2014. Int. J. Nanotechnol. 11 (5–678), 616–625.
Ludwig, K.A., Uram, J.D., Yang, J., Martin, D.C., Kipke, D.R., 2006. J. Neural Eng. 3 (1), 59.
Magri, C., Whittingstall, K., Singh, V., Logothetis, N.K., Panzeri, S., 2009. BMC Neurosci. 10 (1), 81.
Mikulovic, S., Pupe, S., Peixoto, H.M., Do Nascimento, G.C., Kullander, K., Tort, A.B., Leão, R.N., 2016. Neurophotonics 3 (1), 015002.
Nur, R., Matsuhisa, N., Jiang, Z., Nayeem, M.O.G., Ykota, T., Someya, T., 2018. Nano Lett. 18 (9), 5610–5617.
Ochoa, M., Wei, P., Wolley, A.J., Otto, K.J., Ziaie, B., 2013. Biomed. Microdevices 15 (3), 437–443.
Oh, J.Y., Kim, J.Y., Park, C.W., Jung, S.W., Na, B.S., Lee, K., Park, N.M., Lee, S.S., Koo, J.B., Hwang, C.S., 2016. IEEE Electron. Device Lett. 37 (5), 588–590.
Park, J.Y., Chae, H.Y., Chung, C.H., Sim, S.J., Park, J., Lee, H.H., 2010. Soft Matter 6 (3), 677–684.
Park, D.W., Schendel, A.A., Mikael, S., Brodnick, S.K., Richner, T.J., Ness, J.P., Hayat, M.R., Atry, F., Frye, S.T., Pashaie, R., Thongpang, S., Ma, Z., Williams, J.C., 2014. Nat. Commun. 5, 6258.
Park, S.J., Kim, J., Chu, M., Khine, M., 2018. Adv. Mater. Technol. 3 (1), 1700158.
Qi, Y., Kim, J., Nguyen, T.D., Lisko, B., Purohit, P.K., McAlpine, M.C., 2011. Nano Lett. 11 (3), 1331–1336.
Rodríguez-Hernández, J., 2015. Prog. Polym. Sci. 42, 1–41.
Rouse, A.G., Moran, D.W., 2009. In: IEEE Int. Conf. on EMBC. pp. 5514–5517.
Rui, Y., Liu, J., Wang, Y., Yang, C., 2011. Microsyst. Technol. 17 (3), 437.
Sahoo, M., Ramaprabhu, S., 2015. Electrochim. Acta 186, 142–150.
Schweikart, A., Horn, A., Boker, A., Fery, A., 2009. Adv. Polym. Sci. 227, 75–99.
Shi, J., Zhang, H., Snyder, A., Wang, M., Xie, J., Porterfield, D.M., Stanciu, L.A., 2012. Biosens. Bioelectron. 38 (1), 314–320.
Su, Y., Liu, Z., Wang, S., Ghaffari, R., Kim, D.H., Hwang, K.C., Rogers, J.A., Huang, Y., 2014. Int. J. Solids Struct. 51 (7–8), 1555–1561.
Takei, A., Fujita, H., 2015. In: IEEE 28th Int. Conf. on MEMS, pp. 829–832.
Thunemann, M., Lu, Y., Liu, X., Kılıç, K., Desjardins, M., Vandenberghe, M., Sadegh, S., Saisan, P.A., Cheng, Q., Weldy, K.L., Lyu, H., Djurovic, S., Andreassen, O.A., Dale, A.M., Devor, A., Kuzum, D., 2018. Nat. Commun. 9 (1), 2035.
Uddin, A.I., Chung, G.S., 2016. RSC Adv. 6 (67), 63030–63036.
Wang, K., Fishman, H.A., Dai, H., Harris, J.S., 2006. Nano Lett. 6 (9), 2043–2048.
Watanabe, M., Shirai, H., Hirai, T., 2002. J. Appl. Phys. 92 (8), 4631–4637.
Weiland, J.D., Anderson, D.J., 2000. IEEE Trans. Biomed. Eng. 47 (7), 911–918.
Yang, L., Zhao, Y., Xu, W., Shi, E., Wei, W., Li, X., Cao, A., Cao, Y., Fang, Y., 2016. Nano Lett. 17 (1), 71–77.
Yu, C., Masarapu, C., Rong, J., Wei, B., Jiang, H., 2009. Adv. Mater. 21 (47), 4793–4797.
Zhang, J., Liu, X., Xu, W., Luo, W., Li, M., Chu, F., Xu, L., Cao, A., Guan, J., Tang, S., Duan, X., 2018. Nano Lett. 18 (5), 2903–2911.